Contents lists available at ScienceDirect

Translational Oncology

Original Research

The aberrant cancer metabolic gene carbohydrate sulfotransferase 11 promotes non-small cell lung cancer cell metastasis via dysregulation of ceruloplasmin and intracellular iron balance

Wei-Min Chang [a,1], Li-Jie Li [b,c,1], I-An Chiu [d], Tsung-Ching Lai [e], Yu-Chan Chang [f], Hsing-Fang Tsai [c], Chih-Jen Yang [g,h], Ming-Shyan Huang [i], Chia-Yi Su [j], Ting-Lun Lai [k], Yi-Hua Jan [c,*], Michael Hsiao [c,l,m,*]

[a] School of Oral Hygiene, College of Oral Medicine, Taipei Medical University, Taipei, Taiwan
[b] PhD. Program in School of Dentistry, College of Oral Medicine, Taipei Medical University, Taipei, Taiwan
[c] Genomics Research Center, Academia Sinica, Taipei, Taiwan
[d] School of Medicine, College of Medicine, National Yang Ming Chiao Tung University, Taipei, Taiwan
[e] Division of Pulmonary Medicine, Department of Internal Medicine, Wan Fang Hospital, Taipei Medical University, Taipei, Taiwan
[f] Department of Biomedical Imaging and Radiological Sciences, National Yang Ming Chiao Tung University, Taipei, Taiwan
[g] Department of Internal Medicine, Kaohsiung Medical University Hospital, Kaohsiung Medical University, Kaohsiung, Taiwan
[h] School of Post-Baccalaureate Medicine, College of Medicine, Kaohsiung Medical University, Kaohsiung, Taiwan
[i] Department of Internal Medicine, E-Da Cancer Hospital, Kaohsiung, Taiwan
[j] Department of Biomedical Engineering, Johns Hopkins University, Baltimore, MD, USA
[k] Taipei First Girl High School, Taipei, Taiwan
[l] Department and Graduate Institute of Veterinary Medicine, School of Veterinary Medicine, National Taiwan University, Taipei, Taiwan
[m] PhD. Program of Translational Medicine, Taipei Medical University, Taipei, Taiwan

ARTICLE INFO

ABSTRACT

Aberrant metabolism has been proposed as one of the emerging hallmarks of cancer. However, the interplay between metabolic disorders and cancer metastasis remains to be defined. To explore the sophisticated metabolic processes during metastatic progression, we analyzed differentially expressed metabolic genes during the epithelial-mesenchymal transition (EMT) of lung cancer cells and defined the EMT-associated metabolic gene signature in lung adenocarcinoma patients. We found that the glycosaminoglycan (GAG)-chondroitin sulfate (CS) biosynthesis pathway was upregulated in the mesenchymal state of lung cancer and associated with poor prognosis. Notably, carbohydrate sulfotransferase 11 (CHST11), a crucial CS biosynthetic enzyme, was confirmed as a poor prognosis marker in non-small cell lung cancer (NSCLC) by immunohistochemical analysis. Moreover, forced CHST11 expression promoted invasion and metastasis, which was abolished by depleting the final product of CS biosynthesis by chondroitinase ABC treatment or active-domain negative CHST11. *In vivo* metastasis mouse models showed that CHST11 increased lung colonies number and sulfated mucosubstance expression. Furthermore, microarray analysis revealed ceruloplasmin (CP), which facilitated iron metabolism, was the downstream effector of CHST11. CP was upregulated by CHST11 through interferon-γ signaling pathway stimulation and related to unfavorable prognosis. Both forced CP expression and long-term iron treatment increased invasion and lung colony formation. Furthermore, we found 3-AP, an iron chelator, hampered the CHST11-induced metastasis. Our findings implicate that the novel CHST11-CP-iron axis enhances EMT and may serve as a new therapeutic target to treat NSCLC patients.

* Corresponding authors at: Genomics Research Center, Academia Sinica, Taipei, Taiwan.
  E-mail addresses: isaacjan@actgenomics.com (Y.-H. Jan), mhsiao@gate.sinica.edu.tw (M. Hsiao).
[1] These authors contributed equally to this work.

Introduction

In the past few decades, non-small cell lung cancer (NSCLC) has been the most lethal cancer worldwide. There will be an estimated quarter-million newly diagnosed lung cancer cases and 154,050 deaths in the USA [1] and 1.6 million tumor-related deaths worldwide [2]. Surgery and chemotherapy are still the most common lung cancer therapy approaches, but the 5-year lung cancer survival rate is approximately 15% [3]. Recently, tyrosine kinase target therapy and immunotherapy have provided new hope for cancer treatment [4,5]. However, metastasis and recurrence are the most important reasons for lung cancer treatment failure.

Epithelial-mesenchymal transition (EMT) is an initial and essential step for lung cancer metastasis, and it contributes to disease recurrence [6]. Cancer EMT is a dynamic process that allows cancer cells to trans-differentiate from an epithelial phenotype to a mesenchymal phenotype. In lung cancer cell models, EMT can be induced by TGF-β treatment [7, 8]. However, EMT is difficult to capture in patients with cancer because of its brief transition. Salt *et al.* provide an EMT score model that apprises patient EMT status by calculating several gene levels from the transcriptome. The EMT score is the sum of mesenchymal genes (*FN1, VIM, CDH2, ZEB1/2, TWIST1/2*, and *SNAI1/2*) minus the sum of epithelial genes (*CDH1, CLDN4, CLDN7, TJP3*, and *MUC1*) in the transcriptome information. A higher EMT score indicates a higher tendency for mesenchymal status in patients with tumors [9]. Recently, metabolic reprogramming and EMT have been determined to have mutual interactions in cancer progression. However, there is no study focused on the link between EMT status and metabolic gene reprogramming in clinical patients.

Glycosaminoglycans (GAGs) are long-chain unbranched polysaccharides that are major components of proteoglycans in the extracellular matrix and are presented on the cell surface. GAGs consist of repeating disaccharide units linked by glycosidic bonds that create complex structures. GAGs can be categorized into six different families, including chondroitin sulfate (CS), dermatan sulfate (DS), keratan sulfate (KS), heparin, heparan sulfate (HS), and hyaluronan (HA), which are determined by the different core monomeric units [10]. Chondroitin sulfate proteoglycans (CSPGs) are the most prevalent GAGs in the human body and are implicated in many physiological functions, such as morphogenesis, cytokinesis, and neuronal plasticity. In pathological conditions, CSPGs are involved in glial scar formation after brain injury, skeletal disorders, and viral and bacterial infections [11,12]. CS is constructed of disaccharide units of D-glucuronic acid (GlcA) and *N*-acetyl-D-galactosamine (→4GlcAβ1→3GalNAcβ1→) with various modifications to the sulfate groups, making it a highly anionic linear polysaccharide [13] that can be stained with pH 1.0 Alcian blue dye [14]. CS are categorized into six subtypes, namely, CS-A, CS-C, CS-B, CS-D, CS-E, and CS-H, according to the different sulfation sites [15], and the electronegativity of CS promotes its interaction with a variety of biomolecules, such as chemokines, cytokines, growth factors, adhesion molecules, and lipoproteins. CS-A content is increased in malignant mouse osteosarcoma cells compared with benign parental cells [16].

Carbohydrate sulfotransferase 11 (CHST11) is expressed in the Golgi apparatus and catalyzes chondroitin sulfation at the carbon-4 position of *N*-acetylgalactosamine (C4-GalNAc) to form CS-A [17]. C4-GalNAc stimulates the enzyme activity of GalNAc transferase-II, which promotes CS backbone elongation [18] and increases the total CS content. Thus, CHST11 is a crucial enzyme at the beginning of GAG biosynthesis. The enzymatic function and heat stability of CHST11 are highly dependent on *N*-glycosylation at its C-terminal ends [19]. The expression pattern of CHST11 is temporally and spatially specific during mouse embryogenesis [20]. CHST11 is expressed in aggressive breast cancer and multiple myeloma [21,22]. Here, we found that GAG biosynthesis is crucial for NSCLC EMT, especially CHST11, which contributes to cancer progression by changing intracellular iron metabolism.

Materials and methods

Cell cultures

SK-LU-1, NCI-H358, HCC-827, A549, and 293T cells were purchased from the ATCC, cryopreserved in an early passage in liquid nitrogen, and maintained according to standard culture protocols and the manufacturer's instructions. All cells were incubated at 37 °C in the presence of 5% CO_2 in culture media supplemented with 10% FBS (Invitrogen, Waltham, MA, USA) and 1X GlutaMAX™ supplement (Gibco; Thermo Fisher Scientific, Waltham, MA, USA). Long-term treatment with TGF-β (5 ng/ml) or ferric ammonium citrate (FAC, 10 μM) was achieved by co-incubation in culture medium for at least two weeks. All cells were routinely authenticated according to morphologic and growth characteristics, as well as by short tandem repeat (STR) analysis, and confirmed to be free of mycoplasma.

Chemical reagents, antibodies, primers, and vector construction

All chemical reagents, kits, antibody sources, and primer sequences are listed in Supplementary Table S1. CHST11 and CP expression vectors were created by Gateway cloning methods as described in our previous protocol [23]. Briefly, pDONR-CHST11 and pDONR-CP clones were purchased from the DNASU plasmid repository; then, the clones were recombined with the pLenti6.3-DEST vector by LR Clonase II Plus enzyme (Invitrogen, Waltham, MA, USA) and confirmed by Sanger sequencing. Domain-negative CHST11 was designed as previously described [19] and generated from wild-type pDONR-CHST11 by using a GeneArt site-direct mutagenesis kit (Invitrogen, Waltham, MA, USA). Then, the clone was confirmed by Sanger sequencing and recombined with the pLenti6.3-DEST vector by LR Clonase II. Lentivirus was generated from the culture medium of 293T cells transfected with the package vectors, pCMV-Δ R8.91, and pMD.G plasmids, using a calcium phosphate transfection kit. The target cells were obtained from 48 h-viral supernatants infection and further 48 h-antibiotic selection by using 2 μg/ml puromycin or 10 μg/ml blasticidin.

Microarray meta-analysis and cDNA microarray analysis

A549 and NCI-H358 cells were infected with a control or CHST11 vector and then enriched by blasticidin selection. Total RNA was obtained by using a QIAGEN RNeasy mini kit. CHST11-stimulated genes in NSCLC were analyzed by Affymetrix U133 microarray assays and uploaded into the GEO database (GSE131952).

Reporter assay

The pGreenFire SMADs reporter and empty vector vectors were purchased from System Biosciences and packaged into pseudoviral particles in 293T cells. Treated cells (5×10^5) were infected with the SMADs reporter and empty pseudovirus. After an additional 48 h of incubation, the reporter activities were measured by using a Promega One-Glo luciferase assay system. Other common oncogenic reporter vectors (200 ng) were purchased from Promega and transfected into stable NSCLC cells in 24-well plates by Lipofectamine 2000 (Thermo Fisher Scientific, Waltham, MA, USA). The reporter activities were normalized to the intensity of empty control expression in different stable cells.

Ceruloplasmin (CP) ELISA assay

Human CP ELISA kit was purchased from Abcam (AB236718; Cambridge, UK). For the ELISA assays, stable NSCLC cells were seeded into a 6 cm dish. After the cells reached to 80% confluence, the serum-free medium was changed and incubated for another 24 h. Cell debris was removed from the conditioned medium then stored condition

medium at -80 °C. The entire condition medium was measured within one month and following the instruction manual.

Animal studies

All animal experiments were performed in strict accordance with the recommendations of the Guidelines for the Care and Use of Laboratory Animals of the National Health Research Institutes (Miaoli, Taiwan). The protocol was approved by the Institutional Animal Care and Use Committee of the Genomic Research Center, Academia Sinica (Taipei, Taiwan; AS IACUC- 12-02-319). Five- to six-week-old male NOD-SCID gamma (NSG) mice were bred at the Genomic Research Center. The animals were housed in a climate-controlled room (12:12 dark-light cycle, with constant humidity and temperature) with food and water provided *ad libitum*. All efforts were made to minimize suffering. For the lung colony formation assay, 1×10^6 NSCLC A549 stable cells were injected into the tail veins of mice and allowed to grow for 6 weeks or until the first mouse died due to lung cancer-related complications. The lungs were fixed with formalin, and the lung colony numbers were calculated.

Boyden chamber migration and invasion assays

The migration and invasion ability of NSCLC cells were measured by Boyden chamber invasion assay (Neuro Probe Inc, Gaithersburg, MD, USA) as previously described in [24]. Briefly, PVDF coated with 10 μg/mL fibronectin on the lower side was used in the migration assay, and PVDF coated with 1 mg/mL Matrigel Basement Membrane Matrix (BD Biosciences, Franklin Lakes, NJ, USA) on the upper side was used in the invasion assay. In some conditions, cells were pre-treated with chondroitinase ABC for 1 h. A total of 1.5×10^4 cells were seeded into the upper chamber for 14 h (migration) or 16 h (invasion). After fixation, the invaded cells on the membrane were stained with Giemsa stain (Sigma-Aldrich) and then quantified from at least five images obtained through phase-contrast microscopy.

Quantitative reverse transcription PCR (RT-qPCR) assay

The detailed procedure of preformed RT-Q-PCR was described in a previous article [25]. Briefly, the total RNA was extracted from TRIzol reagent (Invitrogen, Waltham, MA, USA) and conducted to RT-PCR by using a SuperScript III kit (Invitrogen, Waltham, MA, USA). The specific gene and amplicon expression levels were detected with OmicsGreen (OmicsBio, Taiwan) and normalized to GAPDH expression. The reaction was performed in 0.1 ml qPCR strip tubes or plates with optical caps or film (Gunster Biotech Co., Taiwan). The primer sequences are shown in Supplementary Table S1.

Western blotting

Cell lysates were kept in lysis buffer, and their concentration was determined by BCA assay (Thermo Fisher Scientific, Waltham, MA, USA). Protein lysates (30 μg) were separated by 10% SDS-PAGE and then electro-transferred to 0.45 μM polyvinylidene difluoride (PVDF) membranes (Merck-Millipore, Burlington, MA, USA). After blocking, the membranes were incubated with primary antibodies at 4 °C overnight, followed by the corresponding secondary antibody for 1 h. The expression signals were visualized using the Immobilon Western Chemiluminescent HRP Substrate (Merck-Millipore, Burlington, MA, USA) and detected using the Fujifilm LAS4000 luminescent image analysis system. The expression was normalized to that of the internal control (β-actin). The antibody dilution conditions are listed in Supplementary Table S1. The original figures of western blotting were deposited in Supplementary File 1.

Sulfotransferase activity

Sulfotransferase activity was detected with the Universal sulfo-transferase activity kit (R&D # EA003) and measured according to the manufacturer's protocol. NSCLC cells were washed twice with normal saline and one time with 1X assay buffer. Then, the cells were lysed in 1% NP-40 in 1X assay buffer and sonicated. Next, 10 μg of total protein lysate was used to measure the sulfotransferase activity.

Total iron assay

Total iron levels were detected using a colorimetric iron assay kit according to the manufacturer's protocol (Sigma #MAK025). Briefly, 2 $\times 10^6$ NSCLC cells receiving different treatments were washed twice with PBS buffer, and the total iron content with reducing agents was measured.

Alcian blue (pH 1.0) staining

An Alcian blue (pH 1.0) kit was purchased from ScyTek Laboratories (Logan, UT, USA). The positively charged Alcian blue staining dye was bound to strongly sulfated glycosaminoglycan with a negative charge and was used to detect the sulfation patterns from mouse lung tissue sections according to the manufacturer's protocol.

Immunohistochemistry

The NSCLC tissue microarray included 125 patients who were diagnosed with NSCLC at the Kaohsiung Medical University Hospital from 1991 to 2007. Three representative 1 mm-diameter cores were taken from each formalin-fixed, paraffin-embedded tumor which had a morphology typical of the diagnosis. CHST11 staining was performed using an automated immunostainer (Ventana Discovery XT Autostainer, Ventana, USA). Antigens were retrieved by heat-induced antigen retrieval for 30 min with TRIS-EDTA buffer. The slides were stained with a polyclonal rabbit CHST11 antibody (1:200; Altas). For CHST11 IHC staining analysis, both the immunoreactivity intensity and percentage were recorded. The intensity of staining was defined as 0, no staining; 1+, weak staining; 2+, moderate staining; and 3+, strong staining. The extent of staining was scored by the percentage of positive cells (0–100%). The final IHC scores (0–300) were the results of multiplying the staining intensity score by the percentage of positive cells. Then, all cases were divided into two groups according to the final IHC scores. A score equal to or greater than 150 was defined as a high IHC expression level, and a score less than 150 was defined as a low expression level. This study was performed with the approval of the Institutional Review Board and with permission from the Ethics Committee of the institution involved (KMUH-IRB-2011-0286).

Immunofluorescence assay

For intracellular iron detection, 1×10^4 A549 cells were seeded on the 18 mm coverslip. Cells were incubated in the dark for one hour with FITC-transferrin (for Fe^{3+}) and FeRhoNox™-1 (for Fe^{2+}) and observed intracellular ferrous or ferric iron content.

Statistical analysis

For *in vitro* and *in vivo* experiments, the statistical analyses were performed using the Student's *t*-test via SPSS (Statistical Package for the Social Sciences) software unless otherwise stated. The figures are created by Prism 7 software (GraphPad Software Inc., La Jolla, CA, USA). Data are presented as the mean ± standard error of the mean (SEM) from three independent experiments. Estimates of the survival rates were calculated by using the Kaplan-Meier method and the log-rank test. Patient follow-up time was censored if the patient was lost

during follow-up. Statistical significance was set at $p < 0.05$ for all our analyses.

Results

Identification of differentially expressed metabolic genes and pathways in lung cancer EMT and their prognostic value among NSCLC patients

The understanding of dynamic interaction between aberrant metabolism and cancer EMT remains elusive. To investigate possible metabolic changes which contributed to lung cancer EMT, we analyzed the microarray datasets (GSE49644 [7]) of TGF-β-induced EMT in three human lung cancer cell lines (A549, NCI-H358, and HCC-827). We first identified 1307 consensus probes that were differentially expressed upon TGF-β induction. Then, we narrowed these down to 216 probes by selecting those with enzyme or transporter annotations. We identified 151 genes as putative EMT metabolic gene signatures (Fig. 1A *left*). Next, we performed cluster hierarchical analysis to visualize the gene expression pattern of putative EMT metabolic gene signatures. As shown in the heat map (Fig. 1A *right*), metabolic genes were differentially expressed between E-type and M-type cancer cells in a consistent manner. To further identify the key metabolic pathways associated with EMT, we conducted KEGG pathway analysis to organize the 151 metabolic genes into pathways and ranked their enrichment according to the significance of the *p*-value (Fig. 1B and Supplementary Table S2). Our analysis suggested that genes in the GAG biosynthesis pathway, including *CHST11, CHSY1, CHPF2, CSGALNACT2,* and *DSE*, were enriched and highly upregulated in the EMT cell model. Furthermore, we analyzed another microarray dataset, GSE31210, that includes 246 tumor samples from lung cancer patients [26] to examine the relationship between metabolic gene expression and patient EMT score [9]. Then, we performed Pearson correlation analyses for EMT scores and metabolic genes in every NSCLC patient and ranked the genes according to the correlation coefficient (R). The orange color indicates $R \geq 0.5$, and the green color indicates $R \leq -0.5$. Interestingly, the most positively correlated genes, *DSE, CHSY1*, and *CHST1*1, also belonged to GAG biosynthesis pathway (Fig. 1C). Then, we used a forest plot to indicate the hazard ratio of individual metabolic genes. As shown in Fig. 1D, the hazard ratios of most candidate genes were greater than 2 or smaller than 0.5. These results indicated that the expression of metabolic genes may serve as a prognostic marker for lung cancer patients. To confirm our findings, we performed Kaplan-Meier survival analyzes by using gene probes from the GAG biosynthesis pathway. Specifically, we found that the upregulation of *CHST11, CHSY1*, and *DSE* was significantly associated with poor survival in the lung cancer patient dataset (GSE31210) (Fig. 1E). Taken together, our observations suggested that metabolic reprogramming, especially the GAG biosynthesis pathway, might contribute to NSCLC EMT and poor prognosis in clinical NSCLC patients.

NSCLC EMT activates GAG biosynthesis pathway

To validate the role of GAG biosynthesis in NSCLC EMT and cancer progression, we used *in vitro* TGF-β treatment or constitutive activation of TGF-β receptor (TGFBR1-T204D) to induce M-type NSCLC cell transformation. TGF-β treatment-induced NSCLC EMT (Fig. 2A) as well as the expression of CHST11, CHSY1, and DSE in A549 and NCI-H358 cells and increased sulfotransferase activity (Fig. 2B and C). TGF-β-induced EMT increased cell migration and invasion abilities. Interestingly, when we depleted cellular surface GAGs with chondroitinase ABC (Chase) treatment or inhibited CS biosynthesis via shRNA knockdown, CHST11 attenuated TGF-β-induced M-type NSCLC metastasis functions (Fig. 2D and Supplementary Fig. 1). Additionally, TGFBR1-T204D also promoted *in vitro* migration and invasion abilities in both A549 and NCI-H358 cells (Fig. 2E and F). Furthermore, TGFBR1-T204D-expressed A549 cells had a more aggressive phenotype, as evidenced by

the *in vivo* lung colony numbers (Fig. 2G and H) and higher levels of strongly sulfated mucosubstance expression (Fig. 2I), which indicated higher chondroitin sulfate content in lung tumors. These results hint that both GAG biosynthesis and its product are crucial for NSCLC progression.

CHST11 serves as a poor prognosis marker in patients with NSCLC

Because CHST11 is an enzyme that not only catalyzes CS-A biosynthesis but also promotes CS backbone elongation [18], we chose CHST11 as a candidate to further investigate GAG biosynthesis in lung cancer progression. Firstly, we performed IHC analysis to confirm CHST11 protein expression and evaluated its prognostic value among patients with NSCLC from Taiwan (Supplementary Table S3). As shown in Fig. 3A, the representative images of CHST11 protein expression in patients with lung cancer. A score of 0 indicates negative CHST11 expression, and a score of 3 indicates the strongest expression. Based on CHST11 protein expression, we determined the prognostic value of the overall survival curve and disease-free survival curve among Taiwan NSCLC patients. An IHC score of 0 and 1 was set as low CHST11 expression, and a score of 2 and 3 was set as high expression. As shown in Fig. 3B, patients with higher CHST11 expression had shorter overall and disease-free survival rates. Furthermore, we validated CHST11 expression in the lung cancer cohort from the Kaplan–Meier Plotter website. The high expression of CHST11 was strongly associated with poor overall survival in lung cancer, especially in lung adenocarcinoma, which has been thought to be the most common subtype of lung cancer in the clinic (Fig. 3C). These results hint that CHST11 may be a poor prognostic marker for NSCLC patients.

CHST11 stimulates GAG content and metastatic cancer potential in vitro and in vivo

To further verify the role of CHST11 in NSCLC, we found ectopic CHST11 expression promoted sulfotransferase activity *in vitro* models (Fig. 4A). Interestingly, CHST11 expression decreased CDH1 reporter activity but induced SMAD4 reporter activity, which indicated that CHST11 upregulated NSCLC EMT (Fig. 4B and C). Moreover, CHST11 expression downregulated the mRNA level and protein expression of E-type marker, CDH1, and upregulated those of M-type markers, such as Slug and Vimentin, which indicated that CHST11 made NSCLC cells undergo EMT (Fig. 4D and E). Also, CHST11 expression stimulated the migration and invasion ability of NSCLC cells. However, the metastasis ability of CHST11 was abolished by an enzyme-inactivated CHST11 (CHST11mt) clone or chondroitinase ABC (Chase) treatment (Fig. 4F–H). Additionally, we used the SK-LU-1 cell line, an M-type NSCLC cell with a high EMT score, to establish a CHST11 knockdown model with two independent shRNA clones (Supplementary Fig. 2A and C). We further determined the metastatic abilities of CHST11 knockdown clones. As shown in Supplementary Fig. 2B–D, CHST11 knockdown increased CDH1 reporter activity, decreased SMAD4 reporter activity, downregulated the protein expression of E-cadherin, and upregulated the protein expressions of Slug as well as Vimentin. Furthermore, CHST11 knockdown significantly reduced the migration and invasion ability of SK-LU-1 cells (Supplementary Fig. 2E and F). These data further confirmed the pro-metastatic ability of CHST11.

Moreover, we examined the effect of CHST11 *in vivo* by intravenous injection into NSG mice. Compared to the control vector, NSG mice with CHST11-expressing A549 cells had higher lung colony numbers (Fig. 4I and J) and more substantial sulfated mucosubstance content in the lungs (Fig. 4K). These results indicate that CHST11 contributes to NSCLC metastasis potential and cancer progression *in vitro* and *in vivo*. Also, CHST11 protein could be a novel poor prognostic marker for NSCLC patients. Our experiments revealed that CHST11 expression was important to NSCLC metastasis and progression.
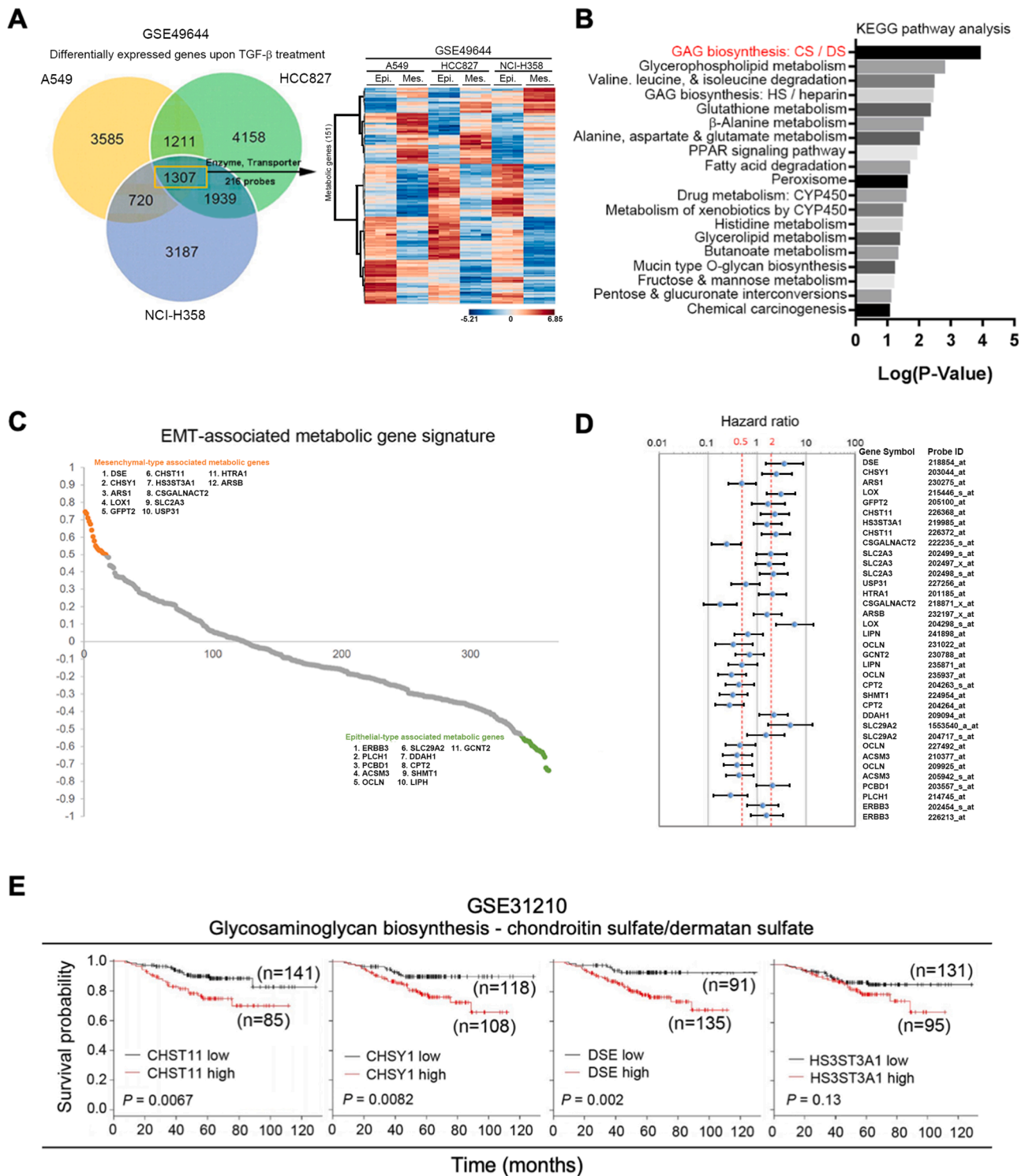
Fig. 1. Both GAG metabolic pathways and genes are highly related to EMT status and prognosis among NSCLC patients.

(A) The *left* panel is a Venn diagram of differentially expressed genes (fold change > 1.5) after TGF-β-induced NSCLC EMT in A549, HCC-827, and NCI-H358 cell lines (GSE49644). There are 1307 differential expression probes from three NSCLC cell lines and 216 probes (151 genes) with enzymes and transporters annotations. The *right* panel is a heatmap of 151 metabolic genes among E-type and M-type NSCLC cells. Red indicates higher expression, and blue indicates lower expression in mesenchymal-type NSCLC cells. (B) KEGG pathway enrichment analysis of EMT-associated metabolic genes. The pathways are ranked according to the -log (*P*-value) by using Fisher's exact test. (C) Pearson correlation analysis between the expression levels of metabolic genes and EMT scores in 246 NSCLC patients (GSE31210). The y-axis indicates the correlation coefficient (R). The orange color indicates $R \geq 0.5$, and the green color indicates $R \leq -0.5$. (D) Forest plot of individual metabolic probe hazard ratios in GSE31210. The dashed lines indicate hazard ratio (HR) = 0.5 or 2. Genes in the GAG biosynthesis pathway were highly correlated with EMT status and poor prognostic values in NSCLC patients. (E) Overall survival analysis of genes belongs to the GAG biosynthesis pathway from the lung cancer microarray dataset (GSE31210) (For interpretation of the references to color in this figure legend, the reader is referred to the web version of this article.).
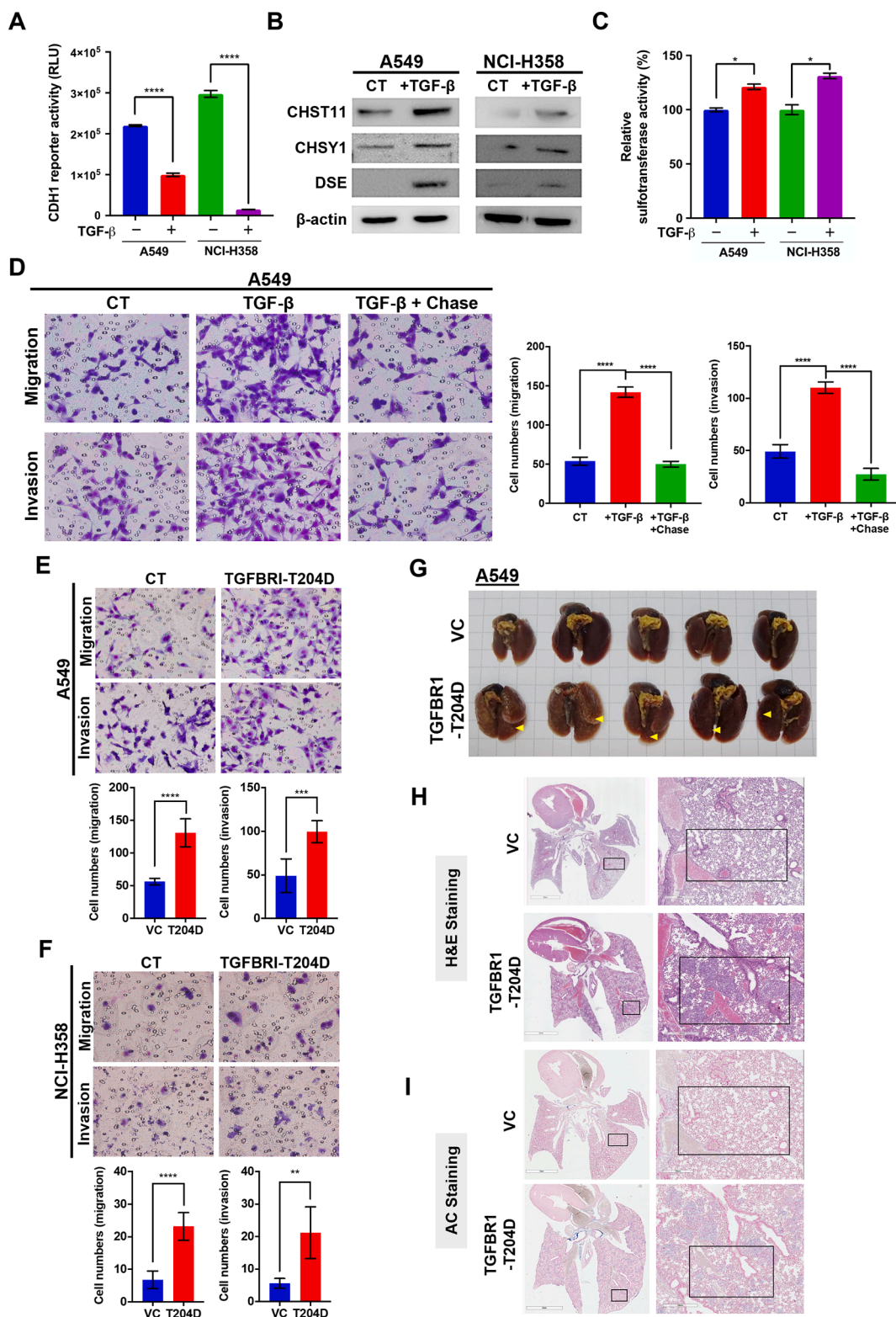
Fig. 2. EMT promotes GAG biosynthesis pathway activation and NSCLC cancer progression.
(A–C) CDH1 reporter assay (A), western blotting of proteins involved in GAG biosynthesis pathway (B), and sulfotransferase activity assay (C) in TGF-β-induced NSCLC EMT models. (D) Boyden chamber migration (*left*) and invasion (*right*) abilities of A549 cells with or without TGF-β or chondroitinase ABC (Chase) treatment. CT, control. (E,F) The metastatic potential induced by the constitutive activation of TGF-β receptor I (TGFBRI-T204D) expression in A549 (E) and NCI-H358 cells (F). The *left* panel is the migration ability, and the *right* panel is the invasion ability. VC, vector control. (G) NSG xenograft lung pictures of A549 cells with or without TGFBR1-T204D expression. Each square indicates 0.5 cm^2. (H,I) Hematoxylin and eosin (H), and Alcian blue (pH 1.0) (I) staining results from (G). In A and C to F, the data represent mean ± SEM derived from three independent experiments. * $p < 0.05$; ** $p < 0.01$; *** $p < 0.001$, compared to control (CT) or vector control (VC) using Student's *t*-test.
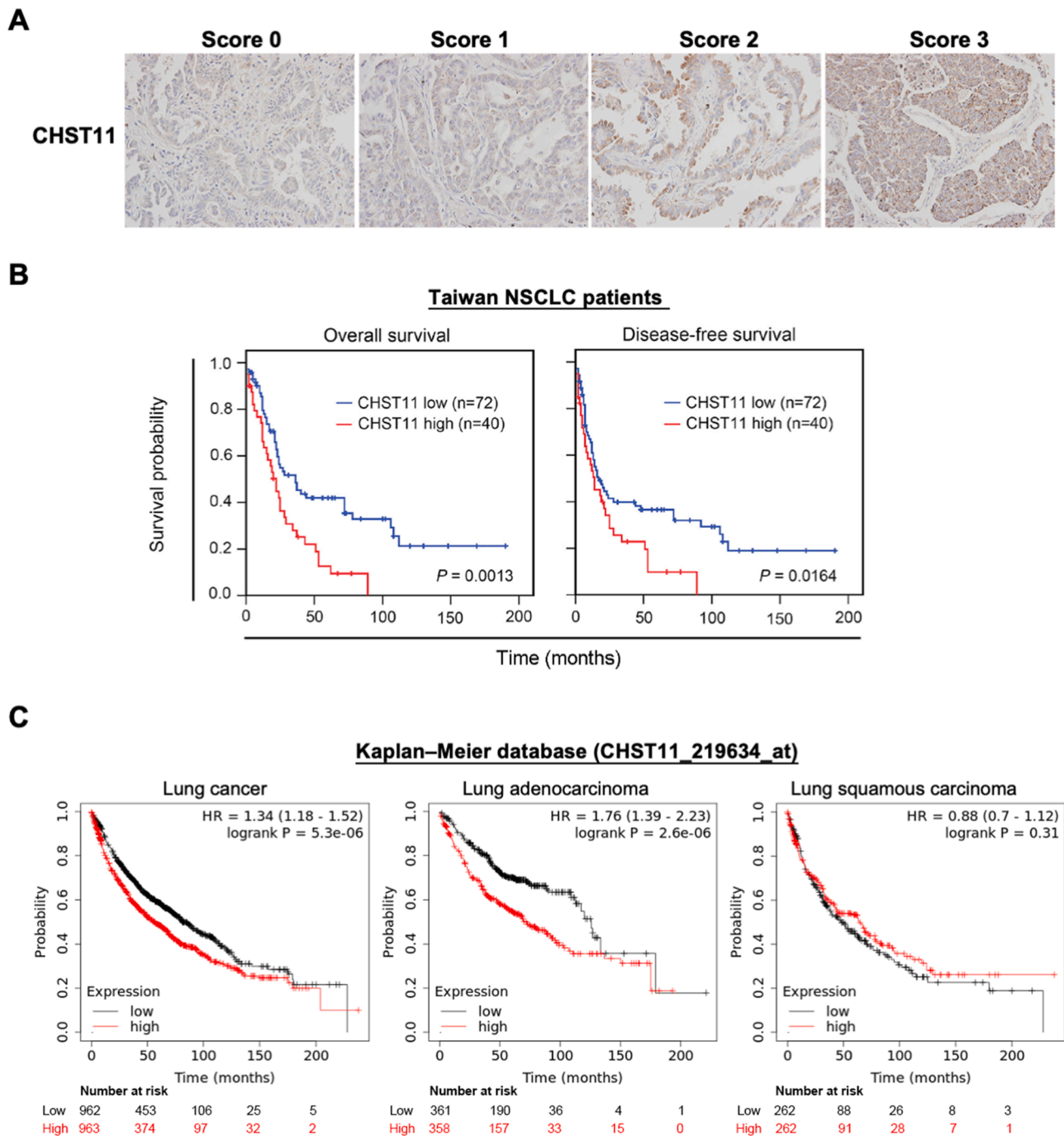
Fig. 3. CHST11 is a poor prognosis marker in clinical NSCLC patients.
(A) Representative IHC images of CHST11 expression in Taiwan NSCLC patients. A score of 0 indicates the weakest CHST11 expression, and a score of 3 indicates the strongest CHST11 expression. (B) Kaplan-Meier plots of CHST11 protein expression at overall survival probability and disease-free survival probability in Taiwan NSCLC patients ($n = 112$) ($p = 0.0013$, $p = 0.0164$, respectively). A score of 0 or 1 was set as patients with low CHST11 expression ($n = 72$), and a score of 2 and 3 was set as patients with high CHST11 expression ($n = 40$). (C) Kaplan-Meier analysis of CHST11 RNA expression at concurrently low or high levels by *in silico* analysis at the endpoint of overall survival probability in patients with lung cancer, lung adenocarcinoma, or lung squamous carcinoma ($p = 5.3e{-}06$, $p = 2.6e{-}06$, $p = 0.31$, respectively). The survival probability was analyzed by using the Gehan-Breslow-Wilcoxon test.

CHST11 stimulates ceruloplasmin expression and intracellular iron homeostasis in NSCLC

To determine the underlying mechanism of CHST11 in NSCLC EMT and cancer progression, we used CHST11 cDNA microarray analysis in both A549 and NCI-H358 cells. The cut-off value was 1.5-fold in CHST11-overexpressing cells compared with that in control cells. There were 314 upregulated and 468 downregulated probes in A549 cells and 316 upregulated and 264 downregulated probes in NCI-H358 cells (Supplementary Table S4). However, only 6 upregulated (*CHST11, CP, TMCO3, NCAM1, TFPI,* and *SCAI*) and 4 downregulated (*SNHG4, DGKH, PRDM9,* and *CNTFR-AS1*) genes overlapped in both cells (Fig. 5A). Ceruloplasmin (CP), which has ferroxidase activity by converting Fe^{2+} into Fe^{3+}, is transported into cells by Fe^{3+}-transferrin [27]. CP was the 2nd highest gene induced by CHST11 in A549 cells and the 71st highest gene induced in NCI-H358 cells (Supplementary Table S4); ectopic
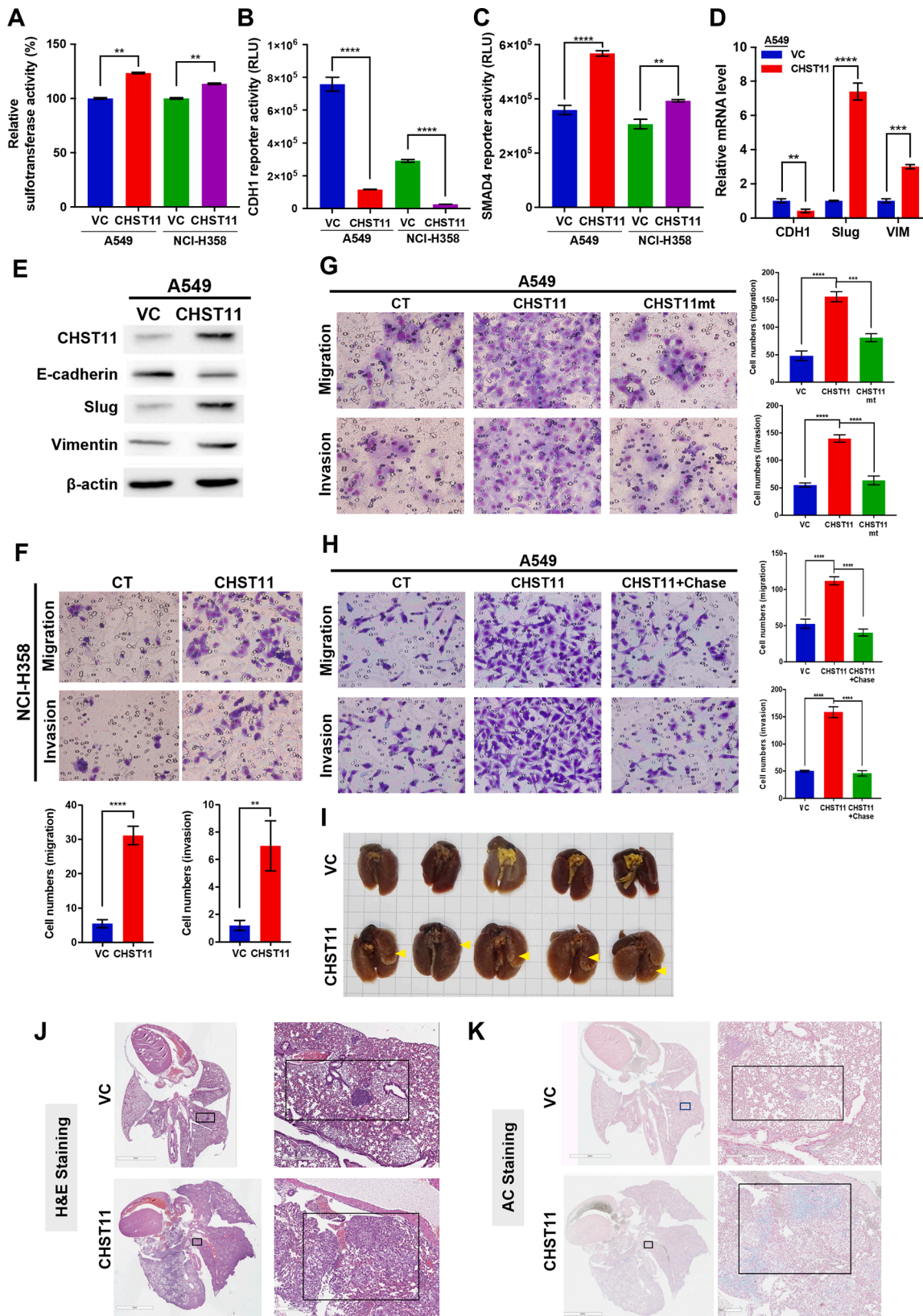
Fig. 4. CHST11 promotes EMT and metastasis potential in NSCLC cells.

(A–C) Sulfotransferase activity (A), CDH1 reporter activity (B), and SMAD4 reporter activity assays of NSCLC cells with or without ectopic CHST11 expression. VC, vector control. (D,E) qRT-PCR (D) and western blotting (E) of CHST11 and EMT markers in A549 cells with or without ectopic CHST11 expression. (F–H) Boyden chamber migration (*left*) and invasion (*right*) abilities of NCI-H358 cells with or without CHST11 expression (F), A549 cells with wild-type CHST11 or enzyme-inactivated clone (CHST11mt) (G), or chondroitinase ABC (Chase) treatment (H). (I) NSG xenograft lung images of A549 cells with or without CHST11 expression. Each square indicates 0.5 cm². (J,K) Hematoxylin and eosin (J) and Alcian blue (pH 1.0) (K) staining results from (I). Data represent mean ± SEM derived from three independent experiments. * $p < 0.05$; ** $p < 0.01$; *** $p < 0.001$, compared to vector control (VC) using Student's *t*-test.
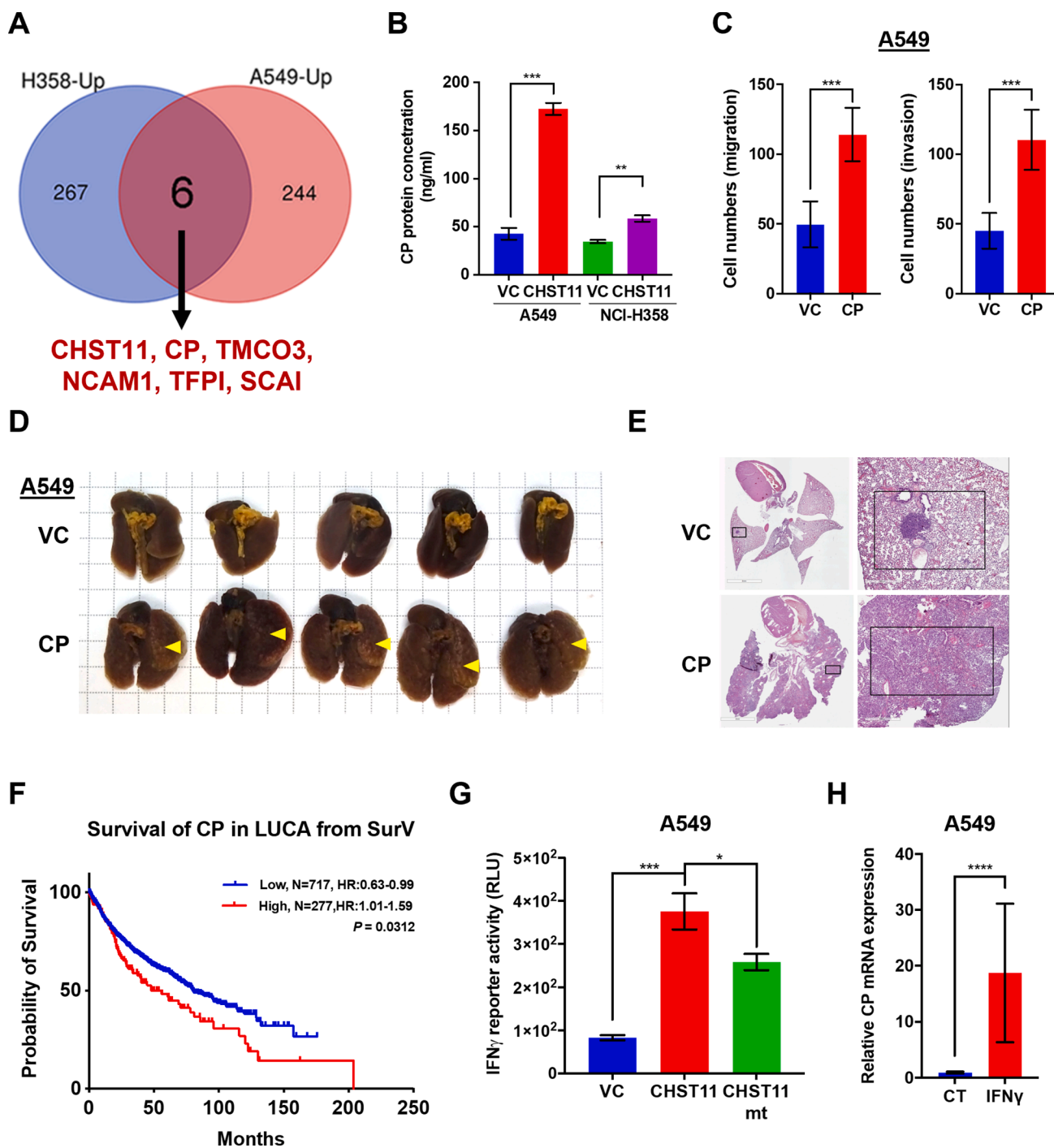
Fig. 5. CP is a key downstream effector in CHST11-induced NSCLC metastasis.
(A) Venn chart of CHST11-activating transcriptomes in A549 and NCI-H358 cells. (B). CP enzyme-linked immunosorbent assay results from both A549 and NCI-H358 cells with or without CHST11 expression. (C) Boyden chamber migration (*left*) and invasion (*right*) abilities of A549 cells with or without CP expression. VC, vector control. (D) NSG xenograft lung images of A549 cells with or without CP expression. Each square indicates 0.5 cm2. (E) Hematoxylin and eosin staining results from (D). (F) Kaplan-Meier analysis of CP mRNA level at the endpoint of overall survival probability in patients with lung cancer ($p = 0.0312$) from the SurvExpres database. (G) IFNγ reporter activity assay of A549 cells with wild-type CHST11 or enzyme-inactivated clone (CHST11mt). VC, vector control. (H) qPCR of CP mRNA levels in A549 cells with or without IFNγ treatment. Data represent mean $\pm$ SEM derived from three independent experiments. * $p < 0.05$; ** $p < 0.01$; *** $p < 0.001$, compared to vector control (VC) or control (CT) using Student's *t*-test. In F, the survival probability was analyzed by using the Gehan-Breslow-Wilcoxon test.

CHST11 expression indeed promoted CP protein levels in both A549 and NCI-H358 cells (Fig. 5B). On the contrary, the CP mRNA level was downregulated in SK-LU-1 cells with shCHST11 (Supplementary Fig. 3). Furthermore, ectopic CP expression significantly promoted *in vitro* NSCLC migration and invasion abilities (Fig. 5C). Also, the ectopic CP expression increased the number of lung colonies in intravenously injected NSG mouse models (Fig. 5D and E). Besides, to investigate the clinical meaning of CP among NSCLC patients, we found CP is a poor prognostic factor according to the lung cancer meta-analysis results from the SurvExpress website (Fig. 5F).

Moreover, to find the potential regulatory mechanism of the CHST11-CP axis, we used ingenuity pathway analysis (IPA) and transcriptome information from the NSCLC cDNA microarray to predict the regulatory network connecting CHST11 and CP. We found that CHST11 might control *CP* mRNA transcription through YWHAE or IFNG (interferon-γ; IFNγ) (Supplementary Fig. 4, Tables S5 and S6). IFNγ reporter activity assay showed ectopic CHST11 expression elevated IFNγ activity, and this activation was partially blocked by enzymatic-inactivated CHST11(Fig. 5G). Furthermore, the IFNγ treatment increased *CP* mRNA levels in A549 cells (Fig. 5H). Therefore, we propose that CP is the major effector of CHST11 in NSCLC EMT, contributes to cancer progression, and is regulated via the IFNγ pathway.

CP-mediated iron imbalance promotes NSCLC progression

CP is the critical protein that oxidizes ferric ions and controls iron homeostasis. Thus, we speculated that the oxidation of ferric ions is involved in CHST11-CP-promoting NSCLC progression. Firstly, we found that the total iron concentration was increased in NSCLC cells with CHST11 overexpression but not in cells with enzymatic death of CHST11 (Fig. 6A). Interestingly, long-term high iron culture with 100 μg/ml ammonium iron (III) citrate stimulated migration and invasion in both A549 and NCI-H358 cells (Fig. 6B). Iron treatment also activated the TGF-β-SMAD promoter and TGF-β-BMP promoter in NSCLC cells by luciferin reporter assay (Fig. 6C and D), which indicated that iron contributed to metastatic potential in NSCLC. Furthermore, we found that the iron chelator, 3-AP, suppressed CHST11-induced NSCLC metastasis (Fig. 6E and F). Unexpectedly, the lung colony formation ability was higher in A549 cells pre-treated with a high iron concentration than in control cells (Fig. 6G and H). Furthermore, CHST11 increased intracellular Fe^{3+}loading more than Fe^{2+}loading in NSCLC cells (Fig. 6I). Consistent with Fig. 6C, the Fe^{3+}-transferrin is a ligand of the transferrin receptor and promotes the master regulator hepcidin through SMAD4 activation [28]. These results suggest that the CHST11-CP-iron axis maintains TGF-β-SMAD/BMP pathway activation and increases the NSCLC metastatic potential after EMT.

Discussion

Here, we demonstrate that chondroitin sulfate biosynthesis pathways are crucial for the NSCLC EMT process and that the activity of the key enzyme CHST11 is critical to the subsequent metastasis potential. In clinical NSCLC patients, CHST11 levels could serve as a poor prognostic marker for both overall and disease-free survival predictions. Because EMT is a transition stage of cancer metastasis, the novel CHST11-CP-iron axis might help maintain metastasis potential in NSCLC cells and promote cancer progression (Fig. 6J). Our study examined aberrant metabolism during EMT and linked iron imbalance to NSCLC progression. Our results shed light on the role of aberrant cancer metabolism in NSCLC metastasis.

GAGs are cellular-size selective barriers that are permselective for cations and other small entitles entering cells. GAG sulfation can be a gatekeeper that prevents extracellular matrix exposure to growth factors (GFs) and maintains cellular cation hemostasis in the microenvironment. Sulfation-free GAGs create stem cell niches saving their host from overexuberant stem cell proliferation due to GF exposure [29,30]. Increasing the cellular GAG sulfation content can increase the binding affinity to GFs and mitogen ligands, such as BMP-2 and WNT-5A [31, 32]. The GAG sulfation patterns are changed in breast [22], colorectal [33], gastric [34], ovarian [35], and prostate [36,37] cancers and promote cancer progression. Our study found that both the CS/DS and HS GAG biosynthesis pathways are upregulated in NSCLC EMT. Moreover, the CS biosynthesis pathway contributes to NSCLC progression. Rangel et al. found that lung cancer tumors have higher GAG sulfation content than adjacent normal lung tissue parenchyma [38]. Patients with highly sulfated GAGs have a shorter overall survival time than those with less sulfated GAGs, which is consistent with our findings and further highlights the role of GAGs in cancer progression.

CHST11 acts as an essential enzyme to initiate the biosynthesis of GAG and the elongation of CS side chains. Previously, aggressive breast cancer cell lines had high CHST11 levels that stimulate P-selectin-mediated adherence to blood vessel endothelial cells and promote metastasis [22]. CHST11 knockout prevents N-cadherin/β-catenin pathway-induced basal-like breast cancer cell invasion [39]. Therefore, these results prove our findings in a lung cancer cell metastasis model. Additionally, CS-A is an enzymatic substrate of CHST11, and it recruits different GFs and morphogens to guide neuron cell migration and bone and cartilage maturation in embryogenesis and bone and cartilage development, respectively [40]. Additionally, CHST11 drives breast cancer aggressiveness by inducing EMT and stem cell-like properties [41]. Besides *CHST11* mRNA levels, the methylation status of this gene has potential as a prognostic biomarker in breast cancer [42]. These points may provide a potential topic for further studies.

Iron is an essential nutrient that is necessary for cell growth and proliferation. Iron content is increased in many different cancer types and promotes cancer progression [28,43,44]. Thus, increasing the iron concentration by CP can also benefit lung cancer cell progression, similar to our findings for CHST11 induction. The crosstalk between EMT-induced aberrant cancer metabolism and iron metabolism may provide new therapeutic niches for blocking metastasis. Recently, 3-AP, the iron chelator, and a ribonucleotide reductase inhibitor have been used in clinical trials for advance stage cancer. However, the response rate is low, and only 25% of treated patients attained stable disease [45,46]. In relapsed NSCLC, combining 3-AP and gemcitabine revealed only a 20% stable-disease rate [47]. Based on our study, 3-AP may be better used in early-stage NSCLC patients than in relapsed patients. Our study might also provide an innovative application of 3-AP by acting as a cancer metastasis inhibitor but not a cancer toxicity agent against lung cancer. In conclusion, our findings highlight the CHST11-CP-iron axis as a pro-metastatic role and CHST11 as a poor prognosis marker among lung cancer, which may provide the potential targeting application against lung cancer metastasis.

Ethics approval and consent to participate

The human subject protocol was performed with the approval of the Institutional Review Board and with permission from the Ethics Committee of the institution involved (KMUH-IRB-2011-0286). The animal studies were approved by the Institutional Animal Care and Use Committee of the Genomic Research Center, Academia Sinica (Taipei, Taiwan; AS IACUC- 12-02-319).
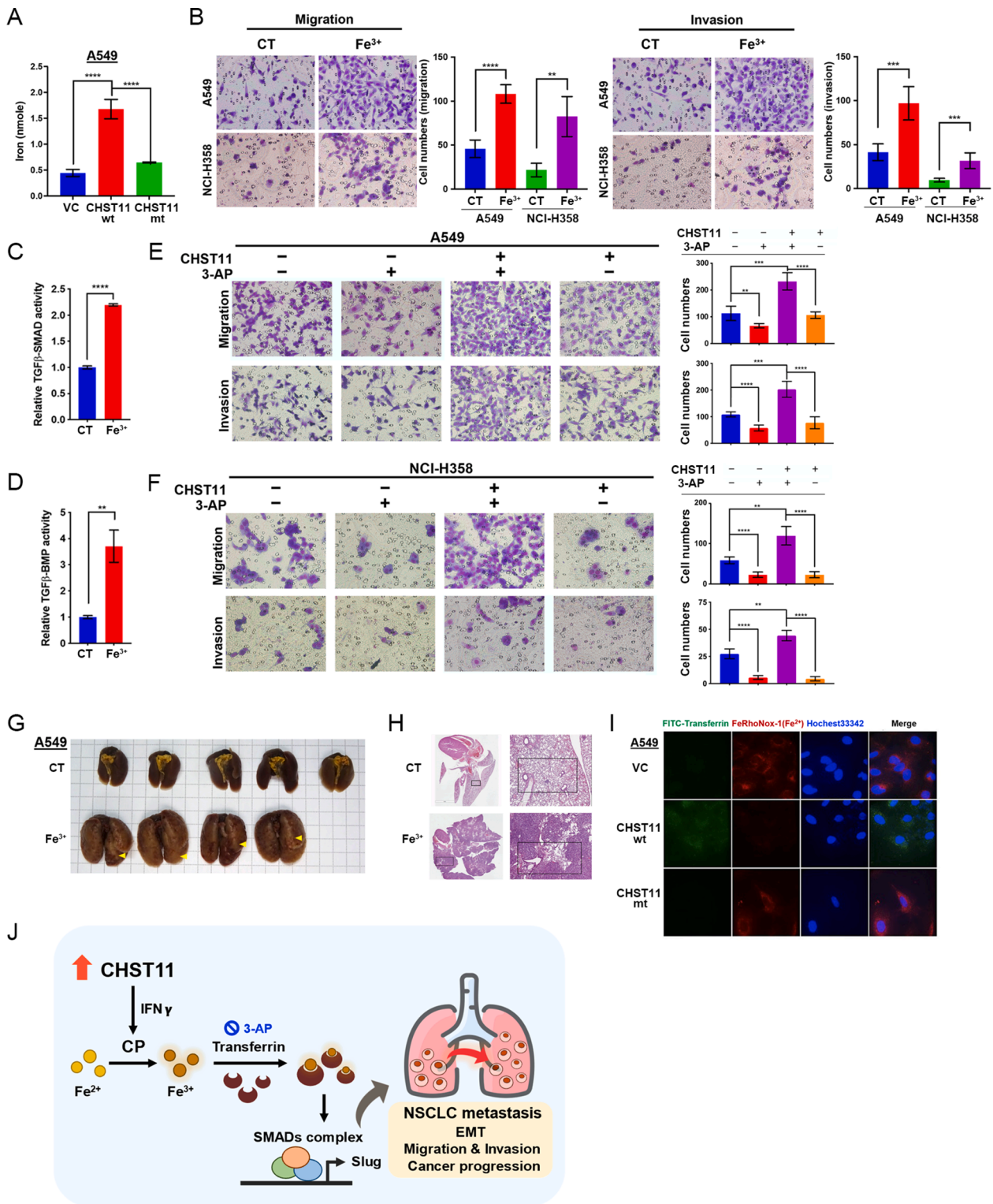
Fig. 6. Iron metabolism is crucial for NSCLC metastasis.

(A) Total iron assays of A549 cells with wild-type CHST11 or enzyme-inactivated clone (CHST11mt). VC, vector control. (B) The *in vitro* NSCLC metastasis potential of A549 cells with or without long-term Fe^{3+} (100 μg/ml) treatment. (C,D) The TGF-β-SMAD reporter (C) and TGF-β-BMP reporter (D) activities of A549 cells with or without long-term Fe^{3+} treatment. (E,F) Boyden chamber metastasis assays for A549 (E) and NCI-H358 (F) cells with or without ectopic CHST11 expression or iron chelator treatment. (G) NSG xenograft lung images of parental or A549 cells with pre-treated with long-term Fe^{3+}. Each square indicates 0.5 cm^2. (H) Hematoxylin and eosin staining results from (G). (I) *In vitro* Fe^{3+} incorporation assay in A549 cells with wild-type CHST11 or enzyme-inactivated clone (CHST11mt). Green indicated FITC-Transferrin, red indicated FeRhoNox-1(Fe^{2+}), and blue indicated nucleus. VC, vector control. (J) Hypothetical model showed the CHST11-CP-iron axis maintains persistent NSCLC metastasis potential. In B, E, F, the left panel is the migration ability, and the right panel is the invasion ability. Data represent mean ± SEM derived from three independent experiments. * $p < 0.05$; ** $p < 0.01$; *** $p < 0.001$, compared to control (VC or CT) using Student's *t*-test.

Consent for publication

All authors approved to publish the study in this journal.

Availability of data and materials

The microarray data were uploaded to the National Center for Biotechnology Information Gene Expression Omnibus (GEO, NCBI, GSE131952). Chemical reagents, vectors, and antibodies are listed in Supplementary Table S1.

CRediT authorship contribution statement

Wei-Min Chang: Conceptualization, Data curation, Methodology, Formal analysis, Writing – original draft, Writing – review & editing. **Li-Jie Li:** Conceptualization, Data curation, Formal analysis, Writing – original draft, Writing – review & editing. **I-An Chiu:** Methodology, Data curation, Writing – original draft. **Tsung-Ching Lai:** Formal analysis, Methodology. **Yu-Chan Chang:** Data curation, Formal analysis, Methodology. **Hsing-Fang Tsai:** Data curation, Methodology. **Chih-Jen Yang:** Resources. **Ming-Shyan Huang:** Data curation, Formal analysis. **Chia-Yi Su:** Formal analysis, Conceptualization. **Ting-Lun Lai:** Formal analysis. **Yi-Hua Jan:** Conceptualization, Data curation, Formal analysis, Supervision, Project administration, Writing – original draft, Writing – review & editing. **Michael Hsiao:** Conceptualization, Supervision, Project administration, Resources, Writing – original draft, Writing – review & editing.

Declaration of Competing Interest

The authors declare that they have no competing interests.

Acknowledgments

Supplementary materials

Supplementary material associated with this article can be found, in the online version, at doi:10.1016/j.tranon.2022.101508.

References

[1] R.L. Siegel, K.D. Miller, A. Jemal, Cancer statistics, 2018, CA Cancer J. Clin. 68 (2018) 7–30.
[2] M. Reck, K.F. Rabe, Precision diagnosis and treatment for advanced non-small-cell lung cancer, N. Engl. J. Med. 377 (2017) 849–861.
[3] N. van Zandwijk, Neoadjuvant strategies for non-small cell lung cancer, Lung Cancer 34 (Suppl 2) (2001) S145–S150.
[4] N.A. Rizvi, S. Peters, Immunotherapy for unresectable stage III non-small-cell lung cancer, N. Engl. J. Med. 377 (2017) 1986–1988.
[5] L. Gandhi, D. Rodriguez-Abreu, S. Gadgeel, E. Esteban, E. Felip, F. De Angelis, M. Domine, P. Clingan, M.J. Hochmair, S.F. Powell, et al., Pembrolizumab plus chemotherapy in metastatic non-small-cell lung cancer, N. Engl. J. Med. 378 (2018) 2078–2092.
[6] A. Singh, J. Settleman, EMT, cancer stem cells and drug resistance: an emerging axis of evil in the war on cancer, Oncogene 29 (2010) 4741–4751.
[7] Y. Sun, A. Daemen, G. Hatzivassiliou, D. Arnott, C. Wilson, G. Zhuang, M. Gao, P. Liu, A. Boudreau, L. Johnson, J. Settleman, Metabolic and transcriptional profiling reveals pyruvate dehydrogenase kinase 4 as a mediator of epithelial-mesenchymal transition and drug resistance in tumor cells, Cancer Metab. 2 (2014) 20.
[8] S.Y. Lee, H.M. Jeon, M.K. Ju, E.K. Jeong, C.H. Kim, M.A. Yoo, H.G. Park, S.I. Han, H.S. Kang, Dlx-2 is implicated in TGF-beta- and Wnt-induced epithelial-mesenchymal, glycolytic switch, and mitochondrial repression by Snail activation, Int. J. Oncol. 46 (2015) 1768–1780.
[9] M.B. Salt, S. Bandyopadhyay, F. McCormick, Epithelial-to-mesenchymal transition rewires the molecular path to PI₃K-dependent proliferation, Cancer Discov. 4 (2014) 186–199.
[10] A. Kowitsch, G. Zhou, T. Groth, Medical application of glycosaminoglycans: a review, J. Tissue Eng. Regen. Med. 12 (2018) e23–e41.
[11] K. Sugahara, H. Kitagawa, Recent advances in the study of the biosynthesis and functions of sulfated glycosaminoglycans, Curr. Opin. Struct. Biol. 10 (2000) 518–527.
[12] K. Sugahara, T. Mikami, T. Uyama, S. Mizuguchi, K. Nomura, H. Kitagawa, Recent advances in the structural biology of chondroitin sulfate and dermatan sulfate, Curr. Opin. Struct. Biol. 13 (2003) 612–620.
[13] A.P. Asimakopoulou, A.D. Theocharis, G.N. Tzanakakis, N.K. Karamanos, The biological role of chondroitin sulfate in cancer and chondroitin-based anticancer agents, In Vivo 22 (2008) 385–389 (Brooklyn).
[14] Y.K. Lee, D.J. Chang, S.K. Chung, A case of Korean patient with macular corneal dystrophy associated with novel mutation in the CHST6 gene, Korean J. Ophthalmol. 27 (2013) 454–458.
[15] F.N. Lamari, N.K. Karamanos, Structure of chondroitin sulfate, Adv. Pharmacol. 53 (2006) 33–48.
[16] M.S. Basappa, K.N. Sugahara, C.M. Lee, G.B. ten Dam, T.H. van Kuppevelt, M. Miyasaka, S. Yamada, K. Sugahara, Involvement of chondroitin sulfate E in the liver tumor focal formation of murine osteosarcoma cells, Glycobiology 19 (2009) 735–742.
[17] S. Yamauchi, S. Mita, T. Matsubara, M. Fukuta, H. Habuchi, K. Kimata, O. Habuchi, Molecular cloning and expression of chondroitin 4-sulfotransferase, J. Biol. Chem. 275 (2000) 8975–8981.
[18] H. Kitagawa, K. Tsutsumi, M. Ujikawa, F. Goto, J. Tamura, K.W. Neumann, T. Ogawa, K. Sugahara, Regulation of chondroitin sulfate biosynthesis by specific sulfation: acceptor specificity of serum beta-GalNAc transferase revealed by structurally defined oligosaccharides, Glycobiology 7 (1997) 531–537.
[19] A. Yusa, K. Kitajima, O. Habuchi, N-linked oligosaccharides are required to produce and stabilize the active form of chondroitin 4-sulphotransferase-1, Biochem. J. 388 (2005) 115–121.
[20] M. Kluppel, The roles of chondroitin-4-sulfotransferase-1 in development and disease, Prog. Mol. Biol. Transl. Sci. 93 (2010) 113–132.
[21] C. Bret, D. Hose, T. Reme, A.C. Sprynski, K. Mahtouk, J.F. Schved, P. Quittet, J. F. Rossi, H. Goldschmidt, B. Klein, Expression of genes encoding for proteins involved in heparan sulphate and chondroitin sulphate chain synthesis and modification in normal and malignant plasma cells, Br. J. Haematol. 145 (2009) 350–368.
[22] C.A. Cooney, F. Jousheghany, A. Yao-Borengasser, B. Phanavanh, T. Gomes, A. M. Kieber-Emmons, E.R. Siegel, L.J. Suva, S. Ferrone, T. Kieber-Emmons, B. Monzavi-Karbassi, Chondroitin sulfates play a major role in breast cancer metastasis: a role for CSPG4 and CHST11 gene expression in forming surface P-selectin ligands in aggressive breast cancer cells, Breast Cancer Res. 13 (2011) R58.
[23] W.M. Chang, Y.F. Lin, C.Y. Su, H.Y. Peng, Y.C. Chang, J.R. Hsiao, C.L. Chen, J. Y. Chang, Y.S. Shieh, M. Hsiao, S.G. Shiah, Parathyroid hormone-like hormone is a poor prognosis marker of head and neck cancer and promotes cell growth via RUNX₂ regulation, Sci. Rep. 7 (2017) 41131.
[24] W.M. Chang, Y.F. Lin, C.Y. Su, H.Y. Peng, Y.C. Chang, T.C. Lai, G.H. Wu, Y.M. Hsu, L.H. Chi, J.R. Hsiao, et al., Dysregulation of RUNX₂/activin-A axis upon miR-376c downregulation promotes lymph node metastasis in head and neck squamous cell carcinoma, Cancer Res. 76 (2016) 7140–7150.
[25] Y.C. Chang, Y.C. Chan, W.M. Chang, Y.F. Lin, C.J. Yang, C.Y. Su, M.S. Huang, A.T. H. Wu, M. Hsiao, Feedback regulation of ALDOA activates the HIF-1alpha/MMP₉ axis to promote lung cancer progression, Cancer Lett. 403 (2017) 28–36.
[26] H. Okayama, T. Kohno, Y. Ishii, Y. Shimada, K. Shiraishi, R. Iwakawa, K. Furuta, K. Tsuta, T. Shibata, S. Yamamoto, et al., Identification of genes upregulated in ALK-positive and EGFR/KRAS/ALK-negative lung adenocarcinomas, Cancer Res. 72 (2012) 100–111.
[27] N.E. Hellman, J.D. Gitlin, Ceruloplasmin metabolism and function, Annu. Rev. Nutr. 22 (2002) 439–458.
[28] B.J. Crielaard, T. Lammers, S. Rivella, Targeting iron metabolism in drug discovery and delivery, Nat. Rev. Drug Discov. 16 (2017) 400–423.
[29] R.A. Smith, K. Meade, C.E. Pickford, R.J. Holley, C.L. Merry, Glycosaminoglycans as regulators of stem cell differentiation, Biochem. Soc. Trans. 39 (2011) 383–387.
[30] L. Gasimli, A.M. Hickey, B. Yang, G. Li, M. dela Rosa, A.V. Nairn, M.J. Kulik, J. S. Dordick, K.W. Moremen, S. Dalton, R.J. Linhardt, Changes in glycosaminoglycan structure on differentiation of human embryonic stem cells towards mesoderm and endoderm lineages, Biochim. Biophys. Acta 1840 (2014) 1993–2003.
[31] V. Hintze, S.A. Samsonov, M. Anselmi, S. Moeller, J. Becher, M. Schnabelrauch, D. Scharnweber, M.T. Pisabarro, Sulfated glycosaminoglycans exploit the conformational plasticity of bone morphogenetic protein-2 (BMP-2) and alter the interaction profile with its receptor, Biomacromolecules 15 (2014) 3083–3092.
[32] M.P. O'Connell, J.L. Fiori, E.K. Kershner, B.P. Frank, F.E. Indig, D.D. Taub, K. S. Hoek, A.T. Weeraratna, Heparan sulfate proteoglycan modulation of Wnt5A signal transduction in metastatic melanoma cells, J. Biol. Chem. 284 (2009) 28704–28712.
[33] D. Kalathas, D.A. Theocharis, D. Bounias, D. Kyriakopoulou, N. Papageorgakopoulou, M.S. Stavropoulos, D.H. Vynios, Alterations of glycosaminoglycan disaccharide content and composition in colorectal cancer: structural and expressional studies, Oncol. Rep. 22 (2009) 369–375.
[34] A.D. Theocharis, D.H. Vynios, N. Papageorgakopoulou, S.S. Skandalis, D. A. Theocharis, Altered content composition and structure of glycosaminoglycans and proteoglycans in gastric carcinoma, Int. J. Biochem. Cell Biol. 35 (2003) 376–390.

[35] A.C. Backen, C.L. Cole, S.C. Lau, A.R. Clamp, R. McVey, J.T. Gallagher, G. C. Jayson, Heparan sulphate synthetic and editing enzymes in ovarian cancer, Br. J. Cancer 96 (2007) 1544–1548.

[36] C. Ricciardelli, K. Mayne, P.J. Sykes, W.A. Raymond, K. McCaul, V.R. Marshall, W. D. Tilley, J.M. Skinner, D.J. Horsfall, Elevated stromal chondroitin sulfate glycosaminoglycan predicts progression in early-stage prostate cancer, Clin. Cancer Res. 3 (1997) 983–992.

[37] C. Ricciardelli, A.J. Sakko, J. Stahl, W.D. Tilley, V.R. Marshall, D.J. Horsfall, Prostatic chondroitin sulfate is increased in patients with metastatic disease but does not predict survival outcome, Prostate 69 (2009) 761–769.

[38] M.P. Rangel, V.K. de Sa, T. Prieto, J.R.M. Martins, E.R. Olivieri, D. Carraro, T. Takagaki, V.L. Capelozzi, Biomolecular analysis of matrix proteoglycans as biomarkers in non small cell lung cancer, Glycoconj. J. 35 (2018) 233–242.

[39] S. Nadanaka, H. Kinouchi, H. Kitagawa, Chondroitin sulfate-mediated N-cadherin/ beta-catenin signaling is associated with basal-like breast cancer cell invasion, J. Biol. Chem. 293 (2018) 444–465.

[40] D. Soares da Costa, R.L. Reis, I. Pashkuleva, Sulfation of glycosaminoglycans and its implications in human health and disorders, Annu. Rev. Biomed. Eng. 19 (2017) 1–26.

[41] A. Behrens, F. Jousheghany, A. Yao-Borengasser, E.R. Siegel, T. Kieber-Emmons, B. Monzavi-Karbassi, Carbohydrate (Chondroitin 4) sulfotransferase-11-mediated induction of epithelial-mesenchymal transition and generation of cancer stem cells, Pharmacology 105 (2020) 246–259.

[42] D. Herman, T.I. Leakey, A. Behrens, A. Yao-Borengasser, C.A. Cooney, F. Jousheghany, B. Phanavanh, E.R. Siegel, A.M. Safar, S. Korourian, et al., CHST11 gene expression and DNA methylation in breast cancer, Int. J. Oncol. 46 (2015) 1243–1251.

[43] S.V. Torti, D.H. Manz, B.T. Paul, N. Blanchette-Farra, F.M. Torti, Iron and Cancer, Annu. Rev. Nutr. 38 (2018) 97–125.

[44] S.V. Torti, F.M. Torti, Iron and cancer: more ore to be mined, Nat. Rev. Cancer 13 (2013) 342–355.

[45] S. Attia, J. Kolesar, M.R. Mahoney, H.C. Pitot, D. Laheru, J. Heun, W. Huang, J. Eickhoff, C. Erlichman, K.D. Holen, A phase 2 consortium (P2C) trial of 3-ami-nopyridine-2-carboxaldehyde thiosemicarbazone (3-AP) for advanced adenocarcinoma of the pancreas, Investig. New Drugs 26 (2008) 369–379.

[46] J.J. Knox, S.J. Hotte, C. Kollmannsberger, E. Winquist, B. Fisher, E.A. Eisenhauer, Phase II study of Triapine in patients with metastatic renal cell carcinoma: a trial of the national cancer institute of canada clinical trials group (NCIC IND.161), Investig. New Drugs 25 (2007) 471–477.

[47] A.M. Traynor, J.W. Lee, G.K. Bayer, J.M. Tate, S.P. Thomas, M. Mazurczak, D. L. Graham, J.M. Kolesar, J.H. Schiller, A phase II trial of triapine (NSC# 663249) and gemcitabine as second line treatment of advanced non-small cell lung cancer: eastern cooperative oncology group study 1503, Investig. New Drugs 28 (2010) 91–97.